Chemistry Europe
European Chemical Societies Publishing

WILEY VCH

Excellence in Chemistry Research

Announcing our new flagship journal

- Gold Open Access
- Publishing charges waived
- Preprints welcome
- Edited by active scientists

Meet the Editors of *ChemistryEurope*

Luisa De Cola
Università degli Studi di Milano Statale, Italy

Ive Hermans
University of Wisconsin-Madison, USA

Ken Tanaka
Tokyo Institute of Technology, Japan

Research Article
doi.org/10.1002/batt.202200509

Chemistry Europe
European Chemical Societies Publishing

www.batteries-supercaps.org

Phase Transformation of VO_2/rGO Composites as High-Voltage Cathodes in Zinc-Ion Batteries

Yuying Li,[a, c] Jingyi Wang,[c] Zhihong Tian,*[a] Feili Lai,[d] Tianxi Liu,[e] and Guanjie He*[b]

Aqueous zinc-ion batteries (ZIBs) are becoming widely concerned candidates as stationary and safe energy storage technology. Vanadium oxides display promising role as cathodes for ZIBs owing to their inherent merits in structures and multiple valence states. However, their unsatisfactory electrical conductivity and narrow voltage window hinder the practical application. Moreover, the charge storage mechanism at the high voltage is unclear. Herein, we synthesized VO_2/rGO composites with high electrical conductivity and demonstrated an electrochemically induced phase transition from tunneled VO_2/rGO to $Zn_3(OH)_2V_2O_7\cdot 2H_2O$/rGO with a laminated structure and an enhanced interlayer spacing during the first charge to 1.6 V, which shows preferable Zn^{2+} storage capacity. Concretely, the electrochemical window of as-assembled ZIB expands to 1.6 V with a specific capacity of 329.9 mAh g^{-1} at 0.1 A g^{-1}, exhibiting wider window compared with the ZIBs based vanadium oxide reported previously. Simultaneously, a long stable lifetime of 84% capacity retention over 1,000 cycles can be recorded. Our work opens a new idea of design strategy to develop high-voltage ZIBs.

Introduction

Developing safe, green, easy manufacturing, and cost-effective energy storage systems is essential for both large-scale stationary and next to the skin devices.[1,2] Recently, the advantages of safe and low toxic characters and natural abundance, make secondary aqueous zinc ion batteries (ZIBs) enticing to researcher.[3–6] Currently, the research interest in cathodes materials, Zn anode and electrolyte for ZIBs are increasing dramatically.[7–9] However, one of the biggest impediments on the road to industrialization of ZIBs is the deficiency of high-performance cathodes.[10,11] Developing suitable cathode materials with high-performance including wide voltage window, superior ion diffusion kinetics and long-life is an urgent task.[12,13]

So far, multiple cathode materials have been synthesized in the laboratory scale after tireless efforts from many academics, such as manganese oxides, vanadium oxides and Prussian blue analogues, exhibiting acceptable reversible Zn^{2+} insertion/extraction behaviors.[14–17] Among them, vanadium oxides are one of the most competitive materials in various battery systems on account of multiple oxidation states (from V^{2+} to V^{5+}) and varied crystalline structures, which allows for more electrons transfer, such as $V_2O_5\cdot nH_2O$,[18] VO_2,[19] $V_3O_7\cdot nH_2O$,[20] $H_2V_3O_8$ nanowires[21] and $NaV_3O_8\cdot 1.5H_2O$.[22] Moreover, previous studies have proven that some vanadium compounds undergo irreversible phase transitions during charge/discharge process.[23,24] Luo et al. investigated the structural evolution of V_2O_3 and the results show a transformation from phase V_2O_3 to phase $V_2O_{5-x}\cdot nH_2O$.

The VO_2 with a tunnel structure (0.82 nm^2, 0.34 nm^2 and 0.5 nm^2 along the *b*-, *a*- and *c*-axis, respectively) is another promising cathode material because it offers an attractive theoretical capacity, which has been calculated as 646 mAh g^{-1}.[25,26] Notwithstanding, the current problems suffered by VO_2 cathodes are their limited electrical conductivity, reduced Zn^{2+} diffusion dynamics, as well as the unclear phase transformation during charge/discharge processes especially with a large voltage window. Carbon-based materials possess high electrical conductivity and stable physicochemical properties.[27,28] To solve the limitation including poor structural stability and conductivity, it has been demonstrated that integrating the cathodes with the carbon-based materials, which possess the high electrical conductivity, such as CNTs and graphene, is an efficient strategy.[29–32]

Herein, we used a convenient and effective strategy for the synthesis of vanadium-based oxides on the surface of graphene oxide with superior conductivity (VO_2/rGO). As demonstrated by the ex-situ experimental analysis, the irreversible phase change occurred in VO_2/rGO composite structures after the first charging process at 1.6 V (Scheme 1), and the in-situ formed

[a] Y. Li, Prof. Z. Tian
Engineering Research Center for Nanomaterials, Henan University Kaifeng 475004, P. R. China
E-mail: zhihong.tian@henu.edu.cn
[b] Prof. G. He
Department of Chemical Engineering, University College London, London WC1E 7JE, U.K.
E-mail: g.he@ucl.ac.uk
[c] Y. Li, J. Wang
School of Chemical Engineering, Zhengzhou University, Zhengzhou 450001, P. R. China
[d] Prof. F. Lai
Department of Chemistry, KU Leuven, Celestijnenlaan 200F, Leuven 3001, Belgium
[e] Prof. T. Liu
Key Laboratory of Synthetic and Biological Colloids, Ministry of Education, School of Chemical and Material Engineering, International Joint Research Laboratory for Nano Energy Composites, Jiangnan University, Wuxi 214122, P. R. China

Supporting information for this article is available on the WWW under https://doi.org/10.1002/batt.202200509

Research Article
doi.org/10.1002/batt.202200509
Chemistry Europe
European Chemical Societies Publishing

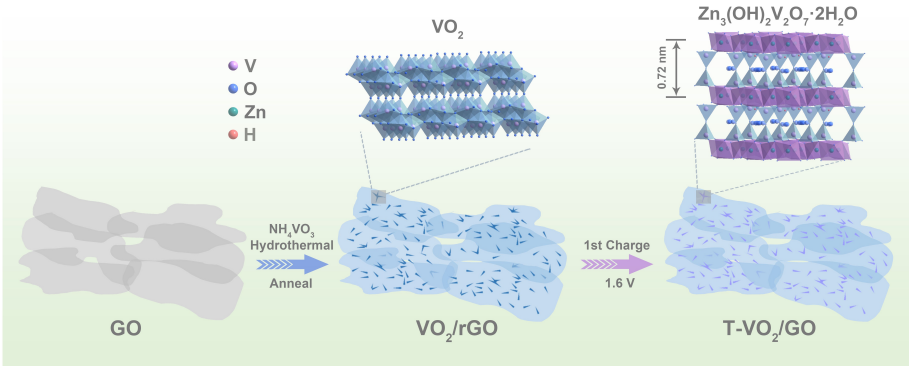

Scheme 1. Fabrication and phase transition process of VO_2/rGO composite.

phase (T-VO_2/rGO) offers better capacity of Zn ion storage and diffusion, making it a competitive cathode candidate for next-generation large-scale ZIBs.

Results and Discussion

The VO_2/rGO composite was produced through two processes. Firstly, the precursor was prepared by a hydrothermal process with graphene oxide (GO) and NH_4VO_3; Next, target products were obtained by an annealing process. In addition, two control materials, i.e., the ones without GO or NH_4VO_3, were prepared.

The phases and structures of as-prepared products were detected by XRD. The peaks of samples without GO can be indexed to the standard V_2O_5 phase (JCPDS-41-1426), as shown in Figure 1(a), and rGO exhibits two characteristic signatures at around 25° and 43°, which are recognized as the (002) and (100) planes of graphitic carbon, respectively.[33] Interestingly, XRD results of the composite nicely match with the monoclinic VO_2 (JCPDS-31-1438), which could be caused by the reduction from the rGO.[26] The morphology of VO_2/rGO composites was observed using SEM and TEM. As illustrated in Figure 1(b and c), VO_2/rGO composite possesses a porous network, and spiny VO_2 structures are on the surface of rGO. As a comparison, SEM images of the V_2O_5 and rGO were also recorded, as shown in Figure S1. TEM and HR-TEM images in Figure 1(d and e) further certify the successful combination of VO_2 and rGO. Furthermore, Figure 1(f) shows the TEM-EDS elemental mappings, indicating that the VO_2/rGO composite contains only C, O and V elements. Based on the Branauer-Emmett-Teller (BET) method, BET surface areas of VO_2/rGO composite is 72.4 $m^2 g^{-1}$ and the pore diameter is concentrated at 5 nm, which could provide large electrochemically active surface areas for charge storage (Figure S2).

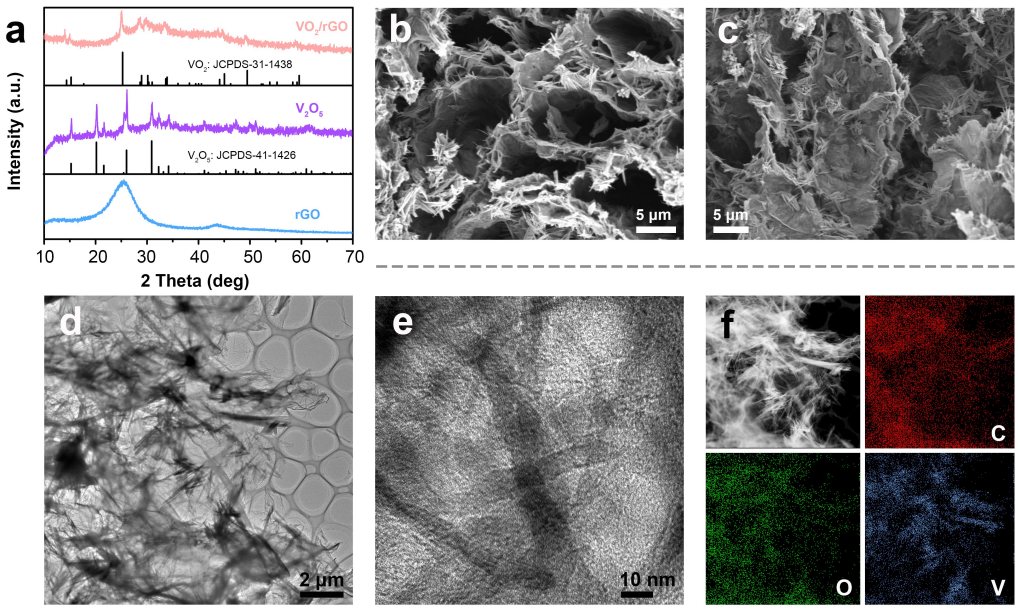

Figure 1. a) XRD patterns. b, c) SEM, d) TEM, e) HRTEM images and f) TEM-EDS elemental mappings of VO_2/rGO.

Research Article
doi.org/10.1002/batt.202200509
Chemistry Europe
European Chemical Societies Publishing

XPS was then used to examine chemical compositions and valence states of VO_2/rGO. Figure 2(a) shows the survey spectra of all samples. Here, sharp peaks in the 284.8, 399.8 and 517.8 eV are associated with C 1s, V 2*p* and O 1s orbitals, respectively. XPS peaks were fitted to provide more information on their structures.[34] Figures 2(b) and (c) show the V 2*p* and O 1s spectra of the V_2O_5 sample respectively. The V element exists the +4 and +5 oxidation states according to the XPS-peak-differentiating analysis. The peaks at 530.7 and 533.3 eV are from O in metal oxide (V–O) and O–H.[35] The C 1s XPS spectrum in Figure 2d shows characteristic peaks of C–C, C–O, V–C and C=O located at 284.8, 285.8, 286.3 and 289.0 eV respectively.[21,35] XPS spectra for V_2O_5 and rGO samples were also provided in Figure S3. The FTIR spectrum of VO_2/rGO composite is shown in Figure 2e to investigate functional groups. It reveals the peak at 505.7 cm^{-1} is result of the symmetric stretching of V–O–V bridges. The peak at 1014.2 cm^{-1} is owing to the stretching vibrations of V=O.[25,34] Besides, the existence of rGO can be proved by peaks observed at 1225.6, 1567.0 and 1734.1 cm^{-1}. Based on the TGA curve in Figure 2(f), the mass proportion of VO_2 in the composite is calculated to be 53.8%.[24] These results further suggest the successful formation of VO_2/rGO composites.

To evaluate the capacity of Zn ion storage and diffusion, as-prepared materials serve as the cathode in CR2032 type coin cells (detail in Electrochemical measurements). The first three CV profiles of VO_2/rGO composite were recorded in Figure 3(a). Remarkably, a strong particular peak located at 1.60 V in the first cycle, while no such phenomenon occurred in the subsequent cycles. Besides, the reduction peaks at approximately 0.48, 0.91 V and the oxidation peaks at about 0.58, 0.96 and 1.18 V can be observed. Meanwhile, GCD curves of VO_2/rGO composites within 0.2–1.6 V are shown in Figure 3(b), and an unexpected beginning charge capacity of 2124.2 mAh g^{-1} can be reached, suggesting that the phase variation process of the VO_2/rGO composite cathode can be achieved within the first charge cycle at ~1.35–1.60 V. After this process, VO_2/rGO composite turns into a new phase (named as T-VO_2/rGO). Figure 3(c and d) shows the CV and GCD curves. Apparently, the current density for T-VO_2/rGO with is larger than VO_2/rGO materials, and T-VO_2/rGO also exhibits a higher discharge capacity of 329.9 mAh g^{-1} at 0.1 A g^{-1}. Additionally, the voltage window of T-VO_2/rGO can reach 1.6 V, which is wider than that of VO_2/rGO (1.35 V). CV curves at different scan rates and GCD curves at different current densities are displayed in Figure S4. The cycling performance of T-VO_2/rGO and VO_2/rGO is evaluated at 5 A g^{-1} for 1,000 continuous cycles in Figure 3(f). It is easily observable that the specific capacity of T-VO_2/rGO is higher than VO_2/rGO for all different cycles, which indicates the structural stability after phase transformation process.

Both electrochemical properties of V_2O_5 and rGO were compared with T-VO_2/rGO. Figure 4a displays rate capabilities for all electrodes. Under various current densities, T-VO_2/rGO composites can achieve average specific capacities of 329.9, 301.4, 278.5, 258.6, 237.4, 211.2, and 163.9 mAh g^{-1} at from 0.1 to 10 A g^{-1}, respectively, which exhibits better Zn ion storage capacity as compared to V_2O_5 and rGO. These results indicate that T-VO_2/rGO composite demonstrates an enhanced rate performance of 54% retention from 0.1 to 10 A g^{-1}. Comparatively, V_2O_5 was only able to demonstrate a 25% retention. The corresponding GCD curves are shown in Figure S5. Figure 4(b) presents the Nyquist plots of T-VO_2/rGO composites and V_2O_5, and T-VO_2/rGO shows a much lower charge-transfer resistance (R_{ct}) of 123 Ω compared with V_2O_5 (279 Ω).[36] The outstanding rate performance and lower charge-transfer resistance for T-VO_2/rGO composite indicates enhanced ion diffusion kinetics.

To further probe satisfactory performances as discussed above, the reaction kinetics of the T-VO_2/rGO composite

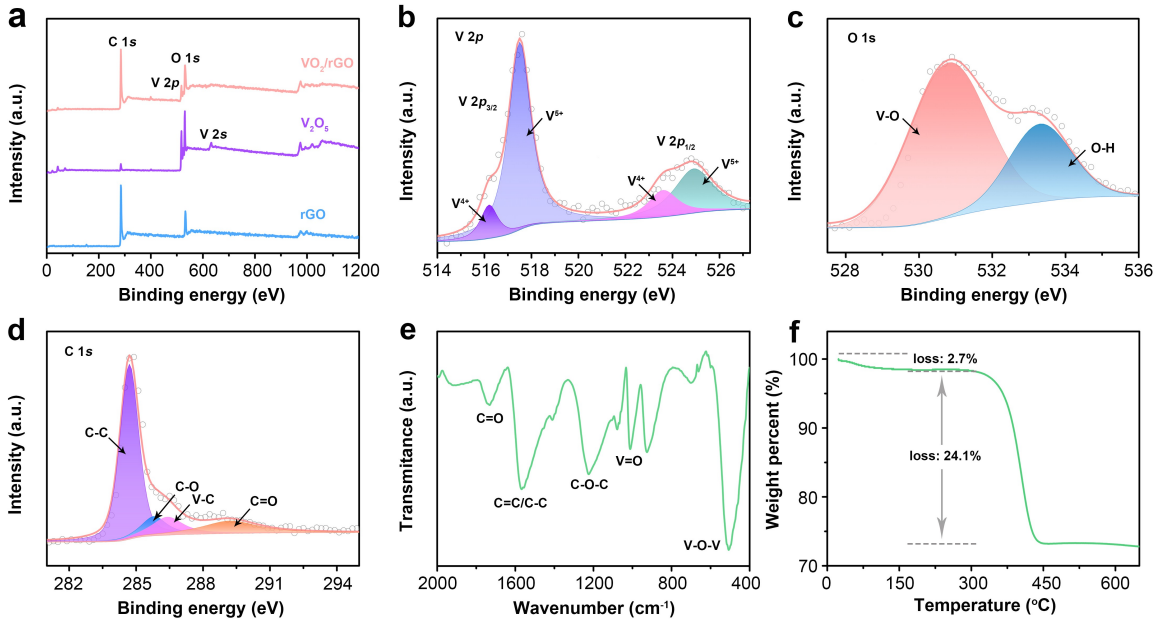

Figure 2. a) XPS survey spectra. b) V 1*p*, c) O 1s and d) C 1s XPS spectra of VO_2/rGO. e) FT-IR spectrum and f) TGA curve of VO_2/rGO.

Research Article
doi.org/10.1002/batt.202200509
Chemistry Europe
European Chemical Societies Publishing

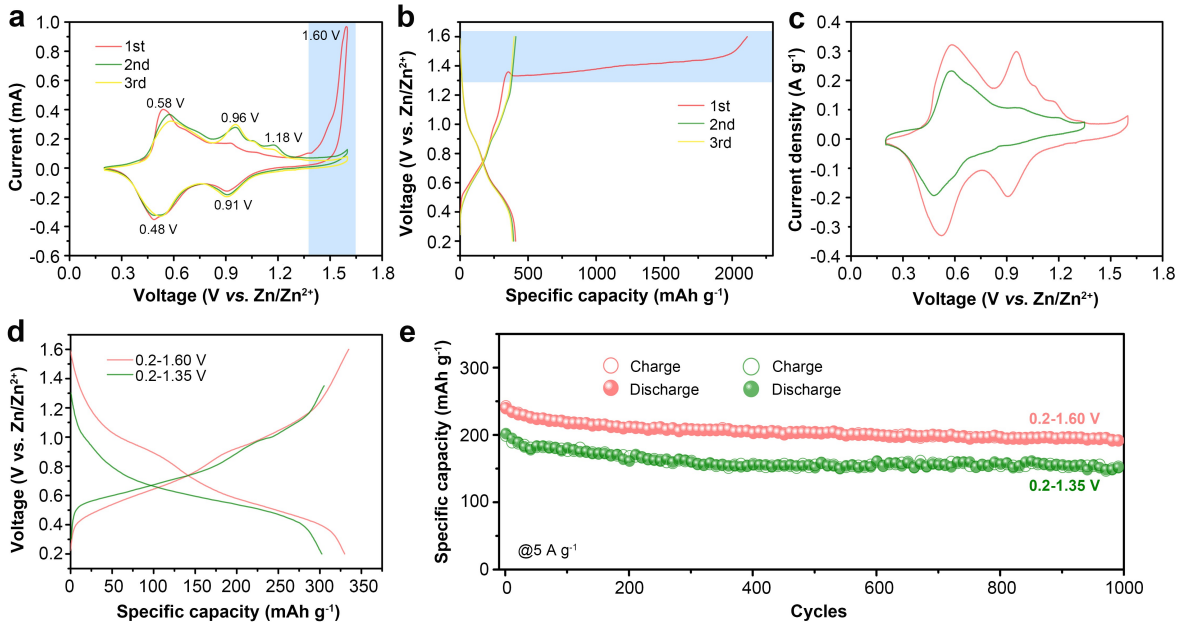

Figure 3. a) CV curves at 0.1 mV s^{-1}, b) GCD curves at 0.1 A g^{-1} of VO_2/rGO of the first three cycles. c) CV curves at 0.1 mV s^{-1}, b) GCD curves at 0.1 A g^{-1}, e) long cycling performance at 5 A g^{-1} of VO_2/rGO with different working windows.

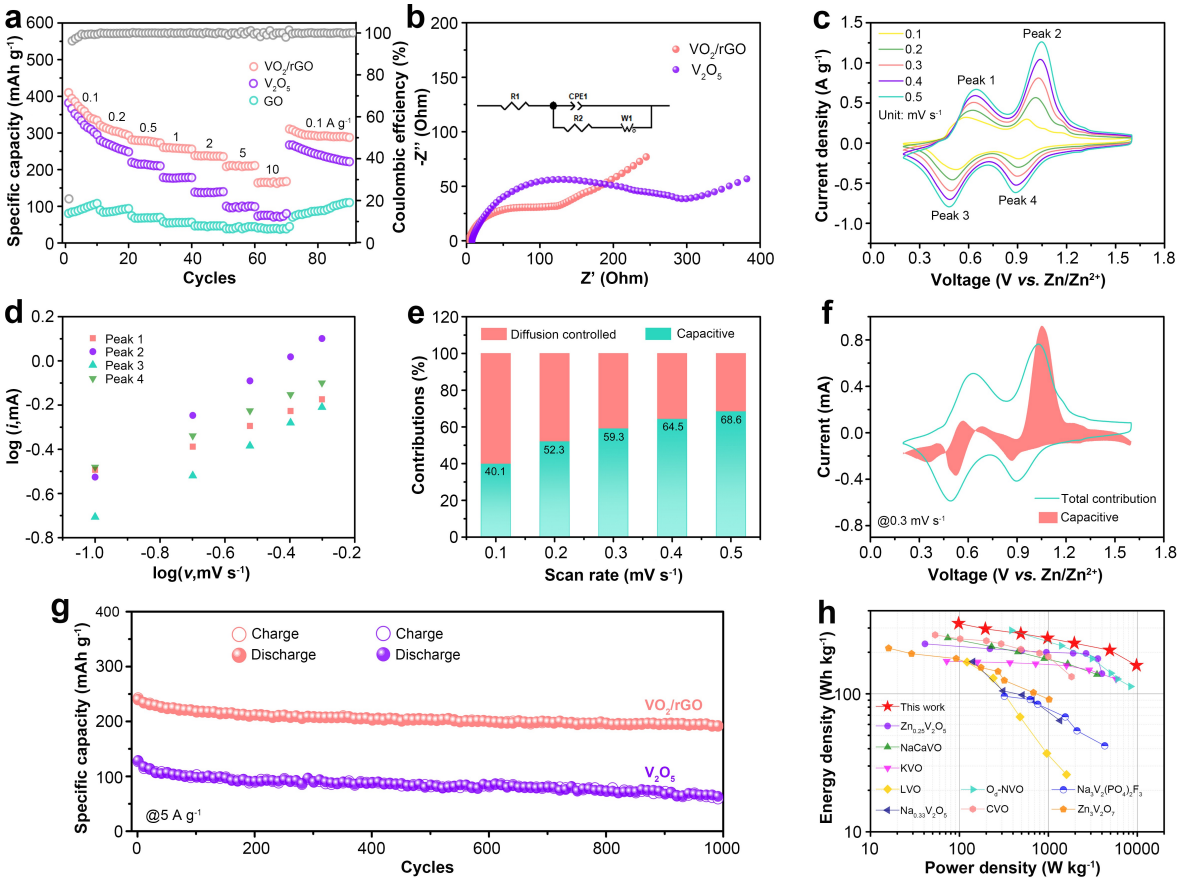

Figure 4. a) Rate performances. b) Nyquist plots. c) CV curves at different scan rates of VO_2/rGO. d) Log(*i*) vs. log(*v*) plots of redox peaks. e) Normalized ratios of the capacitive contribution at different scan rates. f) Diffusion and capacitance contribution at 0.3 mV s^{-1}. g) Cycling performances at 5 A g^{-1} of VO_2/rGO and V_2O_5. h) Ragone plots of VO_2/rGO and other reported ZIBs cathode materials.

Research Article
doi.org/10.1002/batt.202200509
Chemistry Europe
European Chemical Societies Publishing

cathode was evaluated by the kinetic behavior analysis. The CV curves of T-VO_2/rGO, V_2O_5 and rGO cathodes at different scan rates are shown in Figures 4(c) and S6. The CV curves of T-VO_2/rGO suggest a multi-step Zn^{2+} intercalation/deintercalation with two pairs of redox peaks. According to Equations (S1) and (S2), *b* values calculated for the Peak 1, 2, 3 and 4 are found to be 0.51, 0.89, 0.72 and 0.55, respectively, and the range of 0.5–1.0 indicates the electrode simultaneously possesses both capacitive and diffusion processes.[37,38] Figure 4(e) summarizes the capacitive ratios of T-VO_2/rGO cathodes at 0.1–0.5 mV s^{-1} according to Equation (S3), which gradually increases from 40.1% to 68.6%, suggesting an increased dominance of the capacitance-controlled process as the scan rate increases. The shaded region in Figure 4(f) represents the capacitive contribution at 0.3 mV s^{-1}.

The markedly improved structure stability of T-VO_2/rGO can also be verified by long cycling tests at 5 A g^{-1}, and the capacity of T-VO_2/rGO material retains 84% after 1,000 ·ycles. Meanwhile, the Coulombic efficiency is maintained at nearly 100%. Whilst the V_2O_5 cathode shows the capacity retention of 51% after cycling, which indicates rGO plays a key role in stabilizing structure. The T-VO_2/rGO shows a maximum energy/power density of 323.3 Wh kg^{-1}/9,796.3 W kg^{-1}. The superior electrochemical performances of the T-VO_2/rGO electrode are quite competitive, as shown in Figure 4g and Table S1, which is better than those of other reported V-based materials for ZIBs.[32,39–51]

The ex-situ XRD was applied to study different phase compositions of VO_2/rGO electrode under various charge storage states. As discussed above in Figure 5, the characteristic peaks at 14.4° and 15.4° for $VO_2 \cdot nH_2O$ (JCPDS-18-1445) almost disappear completely after the initial charging process to 1.6 V and be never seen again subsequently, which implies the complete variation of phase compositions of $VO_2 \cdot nH_2O$. At full charging state up to 1.6 V, three new weak peaks located at 12.3°, 34.2° and 36.5° appear are assigned to the $Zn_3(OH)_2V_2O_7 \cdot 2H_2O$ (JCPDS-50-0570), indicating the VO_2 of VO_2/rGO electrode transformed into $Zn_3(OH)_2V_2O_7 \cdot 2H_2O$ after the first charging, which may ascribe insertion/extraction of hydrated Zn ion.[24,52] Different from the tunnel-type structure of VO_2, $Zn_3(OH)_2V_2O_7 \cdot 2H_2O$ possesses layered structure and a sufficient interlayer spacing (0.72 nm) to provide enlarged spaces for Zn^{2+} storage and diffusion (Scheme 1).[53] When discharged to 0.2 V, the $Zn_3(OH)_2V_2O_7 \cdot 2H_2O$ signal decreases significantly because of the intercalation of Zn^{2+}. As recharging in the second cycle, the $Zn_3(OH)_2V_2O_7 \cdot 2H_2O$ peaks emerged again, which further proves the irreversible reaction from VO_2/rGO to the product of $Zn_3(OH)_2V_2O_7 \cdot 2H_2O$/rGO (T-$VO_2$/rGO) with a wide voltage window and specific capacity.

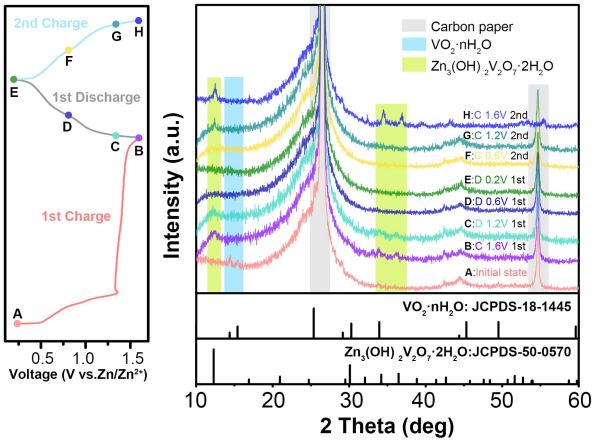

Figure 5. XRD patterns of the cathode at different states.

Conclusion

In summary, the VO_2/rGO composite cathode by a hydrothermal process followed with high temperature treatment for aqueous ZIBs. This compound structure with rGO promotes the high conductivity and stability simultaneously. Moreover, we verify that the irreversible phase variation from VO_2/rGO composite to $Zn_3(OH)_2V_2O_7 \cdot 2H_2O$/rGO (T-$VO_2$/rGO) with layered structure and a large interlayer spacing at the first charging process. Benefitting from the converted structure, the $Zn_3(OH)_2V_2O_7 \cdot 2H_2O$/rGO electrode enables a wide potential window (0.2–1.6 V), a superior specific capacity of 329.9 mAh g^{-1}, an excellent cycling stability (capacity retention of 84% after 1,000 cycles), a high specific energy/power density of 323.3 Wh kg^{-1}/9,796.3 W kg^{-1}, showing promising application as high-voltage vanadium-based cathodes for ZIBs.

Experimental Section

Experimental Section was provided in the Supporting Information.

Acknowledgements

The authors sincerely acknowledge financial support from the National Natural Science Foundation of China (No. 52003251), Henan Center for Outstanding Overseas Scientists (GZS2022014) and Engineering and Physical Sciences Research Council (EPSRC) (EP/V027433/1).

Conflict of Interest

The authors declare no conflict of interest.

Data Availability Statement

The data that support the findings of this study are available from the corresponding author upon reasonable request.

Keywords: high-voltage · phase transition · vanadium oxides · VO_2/rGO composite · zinc-ion batteries

[1] M. A. Hannan, M. M. Hoque, A. Mohamed, A. Ayob, *Renewable Sustainable Energy Rev.* **2017**, *69*, 771–789.
[2] X. Tang, D. Zhou, B. Zhang, S. Wang, P. Li, H. Liu, X. Guo, P. Jaumaux, X. Gao, Y. Fu, C. Wang, C. Wang, G. Wang, *Nat. Commun.* **2021**, *12*, 1–11.
[3] H. Pan, Y. Shao, P. Yan, Y. Cheng, K. S. Han, Z. Nie, C. Wang, J. Yang, X. Li, P. Bhattacharya, K. T. Mueller, J. Liu, *Nat. Energy* **2016**, *1*, 1–7.
[4] W. Li, K. Wang, S. Cheng, K. Jiang, *Adv. Energy Mater.* **2019**, *1900993*, 1–10.
[5] H. Dong, J. Li, J. Guo, F. Lai, F. Zhao, Y. Jiao, D. J. L. Brett, T. Liu, G. He, I. P. Parkin, *Adv. Mater.* **2021**, *33*, 202007548.
[6] T. Zhang, Y. Tang, S. Guo, X. Cao, A. Pan, G. Fang, J. Zhou, S. Liang, *Energy Environ. Sci.* **2020**, *13*, 4625–4665.
[7] T. Wei, Y. Ren, Z. Li, X. Zhang, D. Ji, L. Hu, *Chem. Eng. J.* **2022**, *434*, 134646.
[8] T. Wei, Y. Peng, L. Mo, S. Chen, R. Ghadari, Z. Li, L. Hu, *Sci. China Mater.* **2022**, *65*, 1156–1164.
[9] D. Xu, H. Wang, F. Li, Z. Guan, R. Wang, B. He, Y. Gong, X. Hu, *Adv. Mater. Interfaces* **2019**, *6*, 1–8.
[10] D. Selvakumaran, A. Pan, S. Liang, G. Cao, *J. Mater. Chem. A* **2019**, *7*, 18209–18236.
[11] P. He, Q. Chen, M. Yan, X. Xu, L. Zhou, L. Mai, C. W. Nan, *EnergyChem* **2019**, *1*, 100022.
[12] J. Yan, E. H. Ang, Y. Yang, Y. Zhang, M. Ye, W. Du, C. C. Li, *Adv. Funct. Mater.* **2021**, *31*, 1–30.
[13] E. J. Hansen, J. Liu, *Front. Energy Res.* **2021**, *8*, 1–8.
[14] Y. Lu, T. Zhu, W. Bergh, M. Stefik, K. Huang, *Angew. Chem.* **2020**, *132*, 17152–17159; *Angew. Chem. Int. Ed.* **2020**, *59*, 17004–17011.
[15] D. Chao, W. Zhou, C. Ye, Q. Zhang, Y. Chen, L. Gu, K. Davey, S. Z. Qiao, *Angew. Chem. Int. Ed.* **2019**, *58*, 7823–7828; *Angew. Chem.* **2019**, *131*, 7905–7910.
[16] Q. Zhao, A. Song, S. Ding, R. Qin, Y. Cui, S. Li, F. Pan, *Adv. Mater.* **2020**, *2002450*, 1–25.
[17] Z. Li, T. Liu, R. Meng, L. Gao, Y. Zou, P. Peng, Y. Shao, X. Liang, *Energy Environ. Mater.* **2021**, *4*, 111–116.
[18] M. Yan, P. He, Y. Chen, S. Wang, Q. Wei, K. Zhao, X. Xu, Q. An, Y. Shuang, Y. Shao, K. T. Mueller, L. Mai, J. Liu, J. Yang, *Adv. Mater.* **2018**, *30*, 1–6.
[19] J. Ding, Z. Du, L. Gu, B. Li, L. Wang, S. Wang, Y. Gong, S. Yang, *Adv. Mater.* **2018**, *30*, 2–7.
[20] D. Kundu, S. Hosseini Vajargah, L. Wan, B. Adams, D. Prendergast, L. F. Nazar, *Energy Environ. Sci.* **2018**, *11*, 881–892.
[21] Q. Pang, C. Sun, Y. Yu, K. Zhao, Z. Zhang, P. M. Voyles, G. Chen, Y. Wei, X. Wang, *Adv. Energy Mater.* **2018**, *8*, 1–9.
[22] F. Wan, L. Zhang, X. Dai, X. Wang, Z. Niu, J. Chen, *Nat. Commun.* **2018**, *9*, 1–11.
[23] T. Wei, Q. Li, G. Yang, C. Wang, *J. Mater. Chem. A* **2018**, *6*, 8006–8012.
[24] H. Luo, B. Wang, F. Wang, J. Yang, F. Wu, Y. Ning, Y. Zhou, D. Wang, H. Liu, S. Dou, *ACS Nano* **2020**, *14*, 7328–7337.
[25] X. Liu, G. Xu, Q. Zhang, S. Huang, L. Li, X. Wei, J. Cao, L. Yang, P. K. Chu, *J. Power Sources* **2020**, *463*, 228223.
[26] F. Cui, J. Zhao, D. Zhang, Y. Fang, F. Hu, K. Zhu, *Chem. Eng. J.* **2020**, *390*, 124118.
[27] T. Zhang, Z. Mao, X. Shi, J. Jin, B. He, R. Wang, Y. Gong, H. Wang, *Energy Environ. Sci.* **2022**, *15*, 158–168.
[28] R. Fei, H. Wang, Q. Wang, R. Qiu, S. Tang, R. Wang, B. He, Y. Gong, H. J. Fan, *Adv. Energy Mater.* **2020**, *10*, 1–11.
[29] Z. Wang, Y. Wang, G. Wang, W. Wu, J. Zhu, *J. Energy Chem.* **2021**, *62*, 552–562.
[30] J. Zhang, Y. Huang, Z. Li, C. Gao, S. Jin, S. Zhang, X. Wang, H. Zhou, *Nanotechnology* **2020**, *31*, 375401.
[31] G. Divyapriya, K. K. Vijayakumar, I. Nambi, *Desalination* **2019**, *451*, 102–110.
[32] C. Shen, X. Li, N. Li, K. Xie, J. G. Wang, X. Liu, B. Wei, *ACS Appl. Mater. Interfaces* **2018**, *10*, 25446–25453.
[33] S. S. Karade, S. Lalwani, J. H. Eum, H. Kim, *J. Electroanal. Chem.* **2020**, *864*, 114080.
[34] Y. Lin, F. Zhou, M. Chen, S. Zhang, C. Deng, *Chem. Eng. J.* **2020**, *396*, 125259.
[35] M. Narayanasamy, B. Kirubasankar, M. Shi, S. Velayutham, B. Wang, S. Angaiah, C. Yan, *Chem. Commun.* **2020**, *56*, 6412–6415.
[36] C. Yang, F. Lv, K. Dong, F. Lai, K. Zhao, F. Sun, S. Dou, Q. Wang, J. Xu, P. Zhang, T. Arlt, X. Chen, Y. Chen, I. Manke, S. Guo, *Energy Storage Mater.* **2021**, *35*, 1–11.
[37] Y. Jiao, L. Kang, J. Berry-Gair, K. McColl, J. Li, H. Dong, H. Jiang, R. Wang, F. Corà, D. J. L. Brett, G. He, I. P. Parkin, *J. Mater. Chem. A* **2020**, *8*, 22075–22082.
[38] M. S. Javed, H. Lei, Z. Wang, B. Liu, X. Cai, W. Mai, *Nano Energy* **2020**, *70*, 104573.
[39] C. Xia, J. Guo, Y. Lei, H. Liang, C. Zhao, H. N. Alshareef, *Adv. Mater.* **2018**, *30*, 1–7.
[40] D. Kundu, B. D. Adams, V. Duffort, S. H. Vajargah, L. F. Nazar, *Nat. Energy* **2016**, *1*, 1–8.
[41] C. Xia, J. Guo, P. Li, X. Zhang, H. N. Alshareef, *Angew. Chem. Int. Ed.* **2018**, *57*, 3943–3948; *Angew. Chem.* **2018**, *130*, 4007–4012.
[42] M. H. Alfaruqi, V. Mathew, J. Song, S. Kim, S. Islam, D. T. Pham, J. Jo, S. Kim, J. P. Baboo, Z. Xiu, K. S. Lee, Y. K. Sun, J. Kim, *Chem. Mater.* **2017**, *29*, 1684–1694.
[43] P. He, G. Zhang, X. Liao, M. Yan, X. Xu, Q. An, J. Liu, L. Mai, *Adv. Energy Mater.* **2018**, *8*, 1–6.
[44] W. Li, K. Wang, S. Cheng, K. Jiang, *Energy Storage Mater.* **2018**, *15*, 14–21.
[45] K. Zhu, T. Wu, K. Huang, *Adv. Energy Mater.* **2019**, *9*, 1–12.
[46] J. Li, N. Luo, F. Wan, S. Zhao, Z. Li, W. Li, J. Guo, P. R. Shearing, D. J. L. Brett, C. J. Carmalt, G. Chai, G. He, I. P. Parkin, *Nanoscale* **2020**, *12*, 20638–20648.
[47] P. He, M. Yan, G. Zhang, R. Sun, L. Chen, Q. An, L. Mai, *Adv. Energy Mater.* **2017**, *7*, 1–5.
[48] Y. Cai, F. Liu, Z. Luo, G. Fang, J. Zhou, A. Pan, S. Liang, *Energy Storage Mater.* **2018**, *13*, 168–174.
[49] L. Chen, Y. Ruan, G. Zhang, Q. Wei, Y. Jiang, T. Xiong, P. He, W. Yang, M. Yan, Q. An, L. Mai, *Chem. Mater.* **2019**, *31*, 699–706.
[50] W. Tang, B. Lan, C. Tang, Q. An, L. Chen, W. Zhang, C. Zuo, S. Dong, P. Luo, *ACS Sustainable Chem. Eng.* **2020**, *8*, 3681–3688.
[51] X. Dai, F. Wan, L. Zhang, H. Cao, Z. Niu, *Energy Storage Mater.* **2019**, *17*, 143–150.
[52] Z. Pan, J. Yang, J. Yang, Q. Zhang, H. Zhang, X. Li, Z. Kou, Y. Zhang, H. Chen, C. Yan, J. Wang, *ACS Nano* **2020**, *14*, 842–853.
[53] H. Cao, C. Peng, Z. Zheng, Z. Lan, Q. Pan, U. G. Nielsen, P. Norby, X. Xiao, S. Mossin, *Electrochim. Acta* **2021**, *388*, 138646.

Manuscript received: November 25, 2022
Revised manuscript received: December 25, 2022
Accepted manuscript online: December 26, 2022
Version of record online: January 13, 2023